

Manuscript

“Contribution of Surface Solar Radiation and Precipitation to Spatiotemporal Patterns of Surface and Air Temperature Warming in China from 1960 to 2003” by Jizeng Du et al.

Response to Reviewer # 1

1. Major

Comment: While the regional trend patterns of T_s , T_a , R_s and P and their relations are interesting, the authors did not give fully explanation of the possible reasons causing the formation of these patterns.

Reply: Following the reviewers comments, we added two paragraphs to explain why the changes of R_s and P caused the pattern of T_s and T_a (Lines 120-144):

“It is well known that the diurnal cycles in T_a and T_s are primarily determined by the surface energy budget. After sunrise, the surface absorbs solar radiation, and the surface net radiation becomes positive and heats the surface first. As a result, the air above the surface becomes unstable. Surface net radiation can be partitioned into three parts: ground heat flux, sensible heat flux, and latent heat flux. Ground heat flux heats the surface and stores energy during the daytime, and this energy may be re-emitted at night. Sensible heat flux directly heats the air above the surface. Latent heat flux is the energy employed to vaporize water during the surface water evaporation and vegetation transpiration processes. How surface net radiation partitions into ground heat flux, sensible heat flux, and latent heat flux is determined by both surface and atmospheric conditions (Wang et al., 2010a, b; Wang and Dickinson, 2012), i.e., surface wetness. Daytime surface net radiation is primarily determined by R_s (Wang and Liang, 2008) and precipitation or surface wetness control partition of surface net radiation into latent and sensible fluxes (Wang and Liang, 2008). Therefore, it is expected that changes in R_s and P play a key role in the variability of T_s and T_a (Wild, 2012; Manara et al., 2015; Hartmann et al., 1986).”

However, quantitative assessments of the impact of R_s on T_s and T_a are still lack due

the shortness of high quality of long-term estimates of R_s . In this study, we used sunshine duration derived R_s (Wang, 2014; Wang et al., 2015) to quantitate the impact of R_s on the spatial pattern of T_a and T_s . To our knowledge, this study presents the first analysis of the relationship between R_s (and P) and T_a (and T_s) based on their spatiotemporal patterns and we further quantified the effect of variations of R_s (and P) on T_a (and T_s) in China for the period 1960-2003.”

Comment: Unless I downloaded the wrong version, I found there are some mislabelling of Figures in the text. e.g., I can't find Fig S9g-i (line 383).

Reply: The reviewer has an incorrect version of the supplementary material. The supplementary material has been substantially revised during last revision. We double checked and make sure it is correct in this upload.

Comment: I noticed the authors were asked to justify the calculation of adjusted T , but I can't see the justification in the current version. These parameters (T_a , T_s , R_s and P) interacts with each other, it is not easy to distinguish the casual relations. I am not sure I understand the actual implication of the adjusted T in section 3.3.

Reply: We agree with the reviewer that the regression made in this paper does not provide any information on the casual relation. Following the reviewer's suggestion, we added two paragraphs to explain why the changes of R_s and P impacted the pattern of T_s and T_a (Lines 120-142). The reason is well known, however, the quantitative assessment on this aspect is still lacking because of the shortness of data. Due to continuous effort, we reconstructed long-term time series of surface solar radiation based on the sunshine duration observations. Furthermore, this study first found that the T_s is most suitable parameter to study the issue, which has been ignored by the other researchers. We revised the equations and justifications based on the reviewers' suggestion during last round of review.

2. Minor

Comment: Line 54: Please make Figure or Fig. consistent. E g Figure 1, but Fig. S1.

Reply: We have revised all Figure X to Fig. X in new manuscript.

Comment: Line 22: “stronger in northwest China”. Are you sure it is not the northeast China?

Reply: Thanks for your comments. We agree with you that the warming trend is not only stronger in “northwest China” but also in “northeast China”. So we have corrected this sentence in Line 20-21: “the pattern was stronger in northwest and northeast China and weaker or negative in South China and the North China Plain.”

Comment: Line 22: “and weaker in South China”. Is this before adjust or after adjust? Before adjust as shown in Fig. 4, the trend is negative in South China, not “weaker”.

Reply: This is warming trend before adjusting. We agree with your comments and have corrected this sentence in Line 20-21: “the pattern was stronger in northwest and northeast China and weaker or negative in South China and the North China Plain”.

Comment: Line 23: Rs is redefined as SSR in Fig. S4. Make it consistent.

Reply: The reviewer has the incorrect version of the supplementary material. It is correct in the new version.

Comment: Fig.S6: the caption is copied from the old version; the referenced Figs are not there anymore.

Reply: The reviewer has the incorrect version of the supplementary material. It is correct in the new version.

Comment: Line 28: “were much higher than those in other regions”. It is hard to get this conclusion, since you don’t have enough coverage over other areas.

Reply: Thanks for your comments. We revised this sentence to (Lines 25-27):

“More importantly, the decreasing rates in South China and the North China Plain were stronger than those in other parts of China.”

Comment: Line 32: “North China Plain and the Loess Plateau”. It will be easier to see if you mark these regions on the corresponding map.

Reply: Thanks for your valuable comments. We have marked these regions on the Fig. 9a and introduced them in Line 443-445: “To clearly illustrate these changes, we selected two regions in China for further investigation: R1 primarily included the North China Plain and R2 primarily included the Loess Plateau (see Fig. 9a).”

Comment: Line 92: “sever air pollution “severe air pollution

Reply: We have corrected it in Line 89.

Comment: Line 155: “Our study is the first to use T_s observation as a parameter for identifying regional climate change.” I doubt it.

Reply: We have deleted this sentence in new manuscript.

Comment: Line 196: “reanalyzes”, reanalyses?

Reply: We have revised it in new version.

Comment: Line 241: In Eq (1). Are R_s and P anomalies? Please make it clear.

Reply: Following your comment, we have added a statement that in Line 256-258: “ R_s and P represents the monthly anomalies of surface solar radiation and precipitation respectively”.

Comment: Line 245: “Fig. S3”. Fig. S4?

Reply: The reviewer has the incorrect version of the supplementary material. It is correct for the new version.

Comment: Fig. S4 & 5: Please explain the large difference of the sensitivity in Fig S5a and g.

Reply: We have explained the difference between the sensitivities of T_s and T_a to R_s in Line 339-343: “During the day, T_s is directly determined by the land surface energy

balance, i.e., the incoming energy (including R_s) and atmospheric longwave radiation (Wang and Dickinson, 2013a), and it is partitioned into latent and sensible heat fluxes (Zhou and Wang, 2016). Although T_a is dependent on the land-atmosphere sensible heat flux, it is also affected by local and/or large-scale circulation.”

Comment: Line 342: Fig S7? Please check it is the right Fig.

Reply: The reviewer have the incorrect version of the supplementary material. It is correct for the new version.

Comment: Line 376: Fig. S5? Please check.

Reply: The reviewer has the incorrect version of the supplementary material. It is correct for the new version.

Comment: Line 381-382: Fig S9 doesn't have g-i. Please check.

Reply: The reviewer has the incorrect version of the supplementary material. It is correct for the new version.

Response to Reviewer # 2

1. General Comments

Comment: There is one conceptual issue: the use in L26 and L451 of “caused” for results from the regression analysis between T and R_s . It is not considered acceptable from a regression analysis of A and B to say that A caused B, even though in a simplified surface-boundary layer model, R_s is the primary physical driver of T_{max} . In the real world, other factors (L468) that you have not measured may be involved, and some others such as the outgoing LW are themselves coupled to T_{max} . Your point is that if you use the slope of the partial regression of T_{max} on R_s to remove the spatial variation of R_s , the T_{max} trends became spatially less heterogeneous. Find other wording that allows you to make your point.

Reply: We agree with the reviewer that the regression made in this paper does not

provide any information on the casual relation. Following the reviewer's suggestion, we added two paragraphs to explain why the changes of R_s and P caused the pattern of T_s and T_a (Lines 120-142). The reason is well known, however, the quantitative assessment on this aspect is still lacking because of the shortness of data. Due to the continuous effort, we reconstructed long-term time series of surface solar radiation based on the sunshine duration observations. Furthermore, this study first found that the T_s is most suitable parameter to study the issues, which has been ignored by the other researchers. We revised the equations and justifications based on the reviewers' suggestion during last round of review.

2. Minor

Comment: L92 severe air pollution

Reply: We have corrected it as your comments in new version.

Comment: The notation R_s/P for R_s and P is not conventional as / is normally used for 'divided by'. Also $T_s\text{-max}/ T_a\text{-max}$

Reply: We have replaced all " R_s/P " to " R_s and P ", same to " $T_s\text{-max}/ T_a\text{-max}$ ".

Comment: L278 increased by 0.356 ± 0.0057 °C 0.356 ± 0.057 °C?

Reply: We have revised it in new version.

Comment: L307 This dependence has been successfully attributed to amplified dynamics. This comment needs clarification

Reply: Thanks for your comments. We have changed the expression and make it clearer. "Related studies suggested that this dependence was strongly associated with the mode variability in large-scale circulation, such as a negative trend in the North Atlantic Oscillation during this period (Wallace et al., 2012; Ding et al., 2014)." (Line 324-327).

Comment: L789 which did not include the effect of the R_s variations. Are you sure you

mean this? Or ‘after removing the effect of the R_s variations’ (and P ?)

Reply: Thanks for your comments. We have corrected those sentences: “(c) Annual, warm, and cold seasonal scale trends calculated based on the data before adjusting the effect of R_s and P . (d) Annual, warm, and cold seasonal scale trends calculated based on the data after adjusting the effect of R_s and P .” (Line 815-817).

Comment: L451 ‘primary cause of’ (and L26 of abstract). Find other wording since regression shows correlation and association, but not causes. So it is incorrect to say ‘primary cause’. See also L468-469 where other factors, not measured are mentioned. Reword L326 as well.

Reply: Please see also our response to your general comments. We have revised the wording as your suggestion. “During the study period, R_s decreased by $-1.50 \pm 0.42 \text{ W m}^{-2} 10\text{yr}^{-1}$ in China, which contributed the trends of T_{s-max} and T_{a-max} decreased by about 0.139 and $0.053 \text{ }^\circ\text{C } 10\text{yr}^{-1}$, respectively.” (Line 23-25). “we found that R_s plays a distinctly important role in the spatial warming patterns of T_{s-max} and T_{a-max} ”. (Line 472- 473).

1 **Contributions of Surface Solar Radiation and Precipitation to the Spatiotemporal**
2 **Patterns of Surface and Air ~~Temperature~~ Warming in China from 1960 to 2003**

3 Jizeng Du^{1,2}, Kaicun Wang^{1,2*}, Jiankai ~~Wang~~³Wang², Qian Ma^{1,2}

4 ¹College of Global Change and Earth System Science, Beijing Normal University,
5 Beijing, 100875, China

6 ²Joint Center for Global Change Studies, Beijing 100875, China

7 ³Chinese Meteorological Administration, Beijing, 100081, China

8 **Corresponding author:** Kaicun Wang, College of Global Change and Earth System
9 Science, Beijing Normal University. Email: kcwang@bnu.edu.cn; Tel: +086 10-
10 58803143; Fax: +086 10-58800059.

11

12 **Submitted to Atmospheric Chemistry and Physics**

13 **March ~~15~~17, 2017**

14

带格式的: 字体: Times New Roman

15 **Abstract**

16 Although global warming has been attributed to increases in atmospheric greenhouses
17 gases, the mechanisms underlying spatiotemporal patterns of warming trends remain
18 under debate. Herein, we ~~analysed~~ analyzed surface and air warming observations
19 recorded at 1,977 stations in China from 1960 to 2003. Our results showed a significant
20 spatial pattern for the warming of the daily maximum surface (T_{s-max}) and air (T_{a-max})
21 temperatures, and the pattern was stronger in northwest and northeast China and weaker
22 or negative in South China and the North China Plain. These warming spatial patterns
23 were attributed to surface shortwave solar radiation (R_s) and precipitation (P), which
24 ~~represent the key parameters~~ play a key role of in the surface energy budget. During the
25 study period, R_s decreased by $-1.50 \pm 0.42 \text{ W m}^{-2} 10\text{yr}^{-1}$ in China, which ~~contributed~~
26 ~~reduced~~ the trends of T_{s-max} and T_{a-max} ~~decreased~~ by about 0.139 and 0.053 °C 10yr⁻¹,
27 respectively. More importantly, the decreasing rates in South China and the North China
28 Plain were ~~stronger much higher~~ than those in other ~~study regions~~ parts of China. The
29 spatial contrasts in the trends of T_{s-max} and T_{a-max} in China were significantly reduced
30 after adjusting for the effect of R_s and P . For example, after adjusting for the effect of
31 R_s and P , the difference in the T_{s-max} and T_{a-max} values between the North China Plain
32 and the Loess Plateau was reduced by 97.8% and 68.3%, respectively, the seasonal
33 contrast in T_{s-max} and T_{a-max} decreased by 45.0% and 17.2%, respectively, and the daily

带格式的: 字体: 非加粗

带格式的: 字体: (默认) Times New Roman, 非加粗

带格式的: 字体: 非加粗

带格式的: 字体: (默认) Times New Roman, 非加粗

带格式的: 字体: 非加粗

34 contrast in the warming rates of the surface and air temperature decreased by 33.0%
35 and 29.1%, respectively. This study showed that the land energy budget plays an
36 essential role in the identification of regional warming patterns.

37

38 1. Introduction

39 Increases in observational data and rapid developments in simulation capacity of
40 climate models have provided evidence for the phenomenon of global warming
41 (Hartmann et al., 2013), and the increases in anthropogenic greenhouse gases and other
42 anthropogenic effects are considered as the primary causes. However, significant spatial
43 and temporal heterogeneities in climate warming have been observed. For example,
44 faster warming rates occur in semiarid regions and a “warming hole” has been identified
45 in the central United States (Boyles and Raman, 2003; Huang et al., 2012). These
46 spatiotemporal heterogeneities represent a major barrier to the reliable detection and
47 attribution of global warming (Tebaldi et al., 2005; Mahlstein and Knutti, 2010).
48 Furthermore, uncertainties in model simulations generally increase from global to
49 regional scales because of uncertainty in regional climatic responses to global change
50 (Hingray et al., 2007; Mariotti et al., 2011). Therefore, investigations of the spatial and
51 temporal patterns of regional climate changes and regional climatic response
52 mechanisms to global change are crucial for increasing the accuracy of models designed
53 to detect and explain the causes of global climate change and predictions of future
54 regional climate change.

55 The spatial heterogeneity of climate warming can be attributed to local climate
56 factors and anthropogenic factors (Karl et al., 1991). For the local climate factors,
57 determining factors such as cloud cover and precipitation (P) can significantly influence
58 the speed of regional warming (Hegerl and Zwiers, 2007; Lauritsen and Rogers, 2012).
59 Spatial heterogeneities in climate-factor trends have an important influence on various
60 changes in the land-surface energy balance. Studies have demonstrated that an increase
61 in cloud cover can diminishes the surface solar radiation (R_s) and therefore reduces the
62 daytime temperature (Dai et al., 1997; Zhou et al., 2010; Taylor et al., 2011), although
63 it has the potential to increase night-time temperature by intercepting outgoing
64 longwave radiation (Campbell and VonderHaar, 1997; Shen et al., 2014).

65 Precipitation (P) can alter the proportion of surface absorbed energy partitioned
66 into sensible heat flux and latent heat flux; therefore it has an inevitable effect on both
67 land-surface and near-surface air temperatures (Wang and Dickinson, 2012; Wang and
68 Zhou, 2015). Additionally, P has a significant effect on soil thermal inertia and the
69 response of surface vegetation, which results in an important feedback for regional and
70 global warming (Seneviratne et al., 2010; Wang and Dickinson, 2012; Ait-Mesbah et
71 al., 2015; Shen et al., 2015).

72 In addition to local climate factors, regional climate systems are significantly

73 affected by the anthropogenic emissions of aerosols. Studies have indicated that
74 improvements in air quality in recent decades over North America and Europe have led
75 to brightening effect (Vautard et al., 2009; Wild, 2012), whereas East Asia and India
76 have led to declines in R_s (Xia, 2010; Menon et al., 2002; Wang et al., 2012; Wang et
77 al., 2015). Consequently, variations in R_s may have an effect on both local and global
78 climate change (Wild et al., 2007; Wang and Dickinson, 2013a).

79 Changes in land cover can also alter the energy exchange between the land surface
80 and the atmosphere, and such changes have the potential to affect regional climates
81 (Bounoua et al., 1999; Zhou et al., 2004; Falge et al., 2005). Previous studies have
82 suggested that urbanization and other land-use changes contribute to promoting the
83 warming effect caused by greenhouse gases (Kalnay and Cai, 2003; Lim et al., 2005;
84 Chen et al., 2015). Overall, the effects of these factors on climate change may be very
85 important at the regional scale and could lead to marked spatial differences in regional
86 climate change; however, they are usually omitted from the detection and attribution of
87 climate change at the global scale (Karoly and Stott, 2006).

88 China is a vast territory that has an abundance of climactic zones stretching from
89 tropical to cold temperate, and a special alpine climate is observed over the Tibet
90 Plateau. Additionally, the dramatic economic development and explosive population

91 growth in China in recent decades have caused significant changes in land cover and
92 severe air pollution, including frequent haze events (Yin et al., 2017; Cheng et al., 2014;
93 Wang et al., 2016). The climatic diversity and intensive human activity in this region
94 will likely lead to a unique response to global warming with obvious spatial differences
95 in climate change.

96 Karl et al. (1991) analyzed the observational records for the period 1951–1989
97 and found that warming trends in China were faster than those of the United States but
98 slower than those of the former Soviet Union. Several studies have revealed that the
99 warming rate in Northwest China was approximately $0.33\text{--}0.39\text{ }^{\circ}\text{C }10\text{yr}^{-1}$ during the
100 second half of the last century (Zhang et al., 2010; Li et al., 2012), which was
101 significantly higher than the average warming rate over China of $0.25\text{ }^{\circ}\text{C }10\text{yr}^{-1}$ (Ren
102 et al., 2005) or the average global rate of $0.13\text{ }^{\circ}\text{C }10\text{yr}^{-1}$ (Hegerl and Zwiers, 2007).
103 The air temperature (T_a) over the Tibet Plateau has increased by $0.44\text{ }^{\circ}\text{C }10\text{yr}^{-1}$ over
104 the last 30 years (Duan and Xiao, 2015), and this rate is considerably faster than the
105 overall warming rate in the Northern Hemisphere ($0.23\text{ }^{\circ}\text{C }10\text{yr}^{-1}$) and worldwide
106 ($0.16\text{ }^{\circ}\text{C }10\text{yr}^{-1}$) (Hartmann et al., 2013). To provide insights on global warming and
107 improve the accuracy of future climate change predictions, understanding the
108 characteristics and mechanisms of regional climate change is critical.

109 T_a is a common metric for determining climate change on the global or regional
110 scales. The land surface temperature (T_s) is also important in climate change research
111 because of its direct relationship with the land surface energy budget. Previously, T_s
112 values used in regional climate research are primarily derived from satellite retrievals
113 or reanalysis datasets (Weng et al., 2004; Peng et al., 2014), which both have
114 satisfactory global coverage but questionable accuracy and integrity. Furthermore,
115 satellite-derived T_s values are only available under clear sky conditions, thus limiting
116 their applicability in climate change studies.

117 In China, both T_s and T_a are measured as conventional meteorological observation
118 parameters by nearly all weather stations. An analysis of the spatiotemporal patterns of
119 these parameters identified a close relationship between T_s and T_a , which indicates that
120 T_s and T_a present equivalent accuracy when used to determine the characteristics of
121 climate change. More importantly, T_s is more sensitive than T_a to the local land surface
122 energy budget.

123 It is well known that the diurnal cycles in T_a and T_s are primarily determined by
124 the surface energy budget. After sunrise, the surface absorbs solar radiation, and the
125 surface net radiation becomes positive and heats the surface first. As a result, the air
126 above the surface becomes unstable. Surface net radiation can be partitioned into three

127 parts: ground heat flux, sensible heat flux, and latent heat flux. Ground heat flux heats
128 the surface and stores energy during the daytime, and this energy may be re-emitted at
129 night. Sensible heat flux directly heats the air above the surface. Latent heat flux is the
130 energy employed to vaporize water during the surface water evaporation and vegetation
131 transpiration processes. How surface net radiation partitions into ground heat flux,
132 sensible heat flux, and latent heat flux is determined by both surface and atmospheric
133 conditions (Wang et al., 2010a; Wang et al., 2010b; Wang and Dickinson, 2012), i.e.,
134 surface wetness. Daytime surface net radiation is primarily determined by ~~Both~~ R_s
135 (Wang and Liang, 2008) and precipitation or surface wetness control partition of surface
136 net radiation into latent and sensible fluxes (Wang and Liang, 2008). Therefore, it is
137 expected that changes in R_s and P play a key role in the variability of T_s and are key
138 factors controlling the land surface energy budget; therefore, changes in these two
139 factors most likely cause regional differences in the warming rate of T_a (Hartmann et
140 al., 1986; Wild, 2012; Manara et al., 2015).

141 However, quantitative assessments of the impact of R_s on T_s and T_a are still lack
142 due the shortness of high quality of long-term estimates of R_s . In this study, we used
143 sunshine duration derived R_s (Wang, 2014; Wang et al., 2015) to quantitate the impact
144 of R_s on the spatial pattern of T_a and T_s . To our knowledge, this study presents the first
145 analysis of the relationship between R_s (and P) and T_a (and T_s) based on their

带格式的: 字体: 非倾斜

带格式的: 字体: 倾斜

带格式的: 字体: 倾斜, 下标

带格式的: 字体: 倾斜

带格式的: 字体: 倾斜, 下标

带格式的: 字体: 倾斜

带格式的: 字体: 倾斜, 下标

146 spatiotemporal patterns and we further quantified the effect of variations of R_s (and P)
147 on T_a (and T_s) in China for the period 1960–2003.

148 This article is organized as follows. Section 2 introduces the data and methods
149 used in the study. Section 3 describes the spatial and temporal patterns of climate
150 warming over China, analyses the effect of the variation in R_s and P on T_a and T_s , and
151 examines the spatial and temporal patterns of the warming trend of T_a and T_s after
152 adjusting for the effects of R_s and P , which eliminated the effects of R_s and P on
153 warming and highlighted the effects of large-scale warming caused by elevated
154 concentrations of atmospheric greenhouse gases. Moreover, the spatial contrast in the
155 warming trends of T_a and T_s in China was substantially reduced after adjusting for the
156 effect of R_s and P , and this result is consistent with the expectations under global
157 warming. Finally, Section 4 presents a summary and discussion.

158 **2. Data and methods**

159 **2.1. Data**

160 The meteorological observational data used in this study are included recently
161 released daily meteorological datasets, such as the China National Stations'
162 Fundamental Elements Datasets V3.0 (CNSFED V3.0), and they were downloaded

163 from China's National Meteorological Information Centre (<http://data.cma.gov.cn/data>)
164 (Cao et al., 2016). These datasets included observations of T_s , T_a , barometric pressure,
165 relative humidity, and sunshine duration. All of the observational records of the climate
166 variables were subjected to quality control measures, and the data acquisition and
167 compilation.

168 As shown in Fig. 1, the number of stations used in this study (1,977 stations
169 selected from a total of 2,479 stations) was significantly higher than that of previous
170 studies (i.e., 57–852 stations) (Kukla and Karl, 1993; Shen and Varis, 2001; Liu et al.,
171 2004; Li et al., 2015). Therefore, the observational data provided better spatial coverage
172 and higher confidence in the detection of regional climate change than in previous
173 studies (Fig. 1).

174 Observations of T_s from weather stations are different from T_s data retrieved via
175 other approaches, such as satellite images and reanalysis. The T_s observations were
176 performed in 4×2 m square bare land plots proximal to the weather stations. The
177 surface of the observational fields was loose, grassless and flat, and at the same level
178 as the ground surface of the weather station. Three thermometers, including a surface
179 thermometer, a surface maximum thermometer, and a surface minimum thermometer
180 were placed horizontal to the surface of the observational field, with half of each

181 thermometer embedded in the soil and the other half exposed to the air. When the
182 observational field was covered by snow, the thermometers were placed on the snow
183 surface. Additionally, the exposed parts of the thermometers were cleaned to remove
184 dust and dew.

185 We verified the reliability of the T_s observational records by analyzing the
186 relationship between T_a and T_s during 1960–2003. As shown in Fig. S1, the mean
187 Pearson ~~Correlation~~correlation ~~Coefficients~~coefficients between daily maximum land
188 surface temperature (T_{s-max}) and daily maximum air temperature (T_{a-max}) calculated
189 from the monthly anomalies were 0.775, 0.843, and 0.806 for the annual, warm, and
190 cold seasonal scales, respectively, and these values were statistically significant (99%
191 confidence level) for all stations. The mean correlation coefficients between the daily
192 minimum land surface temperature (T_{s-min}) and daily minimum air temperature (T_{a-min})
193 were 0.861, 0.842, and 0.865 for the annual, warm, and cold seasonal scales,
194 respectively, and these values were statistically significant (99% confidence level) for
195 all stations. The high correlations indicated that observations of either T_s or T_a could be
196 used for climate change detection.

197 The most fundamental energy resource for T_s and T_a is R_s . In most previous studies,
198 the observed R_s have been used to analyze the relation between the variation in R_s and

带格式的: 字体: 倾斜

199 T_a over China. However, fewer sites were used for R_s observations than for other
200 climatic variables; for example, only 85 sites were used for R_s observations in Liu et al.
201 (2004) and only 90 sites were used in Li et al. (2015).

202 Importantly, sensitivity drift the instruments used for the R_s observations led to a
203 faster dimming rate before 1990, and instrument replacements from 1990 to 1993
204 resulted in a false sharp increase in R_s (Wang, 2014; Wang et al., 2015). The limited
205 distribution and low quality of R_s observations have impeded the wide scientific
206 application of this parameter.

207 Therefore, we used sunshine duration-derived R_s , which is based on an effective
208 hybrid model developed by Yang et al. (2006). This model has subsequently been
209 improved (Wang, 2014; Vose et al., 2005) and it has performed well in regional and
210 global applications (Tang et al., 2011; Wang et al., 2012). Sunshine duration-derived
211 R_s not only accurately reflects the effects of clouds and aerosols on the R_s but also more
212 exactly reveals long-term trends (Wang, 2014; Wang et al., 2015). Additionally,
213 sunshine duration-derived R_s values are better correlated with the satellite retrievals,
214 reanalysis, and climate model simulations than R_s values observed from observation
215 (Wang et al., 2015)(Wang et al., 2015a).

216 The data are collected by a total of 2,474 meteorological stations; however, the

217 lengths of the effective observation records for the stations are different. Additionally,
218 only a small number of stations were installed before 1960, and the observational
219 records of T_s at many stations were anomalous after 2003 because of automation.
220 Therefore, in our analysis, we selected 1,977 meteorological stations (see Fig. 1) for
221 which the observation records with valid data were longer than 30 years during the 43
222 years between 1960 and 2003.

223 The monthly anomalies relative to the 1961–1990 climatology were calculated
224 based on a monthly mean value of the daily values, and when a month was missing
225 more than 7 daily values, that month was classified as a missing value (Li et al., 2015;
226 Sun et al., 2016). For the annual anomalies, the monthly anomalies were averaged for
227 the entire year. The anomalies in the warm seasons were the averages of the monthly
228 anomalies from May to October, and the anomalies in the cold seasons were the
229 averages of the monthly anomalies from November to the next April.

230 **2.2 Methods**

231 As shown in Fig. 1, the spatial distribution of the weather stations throughout
232 China is extraordinarily asymmetric and the density of weather stations in east China is
233 far greater than that in west China. We used the area-weight average method to reduce
234 these biases when calculating the national mean. First, we divided the study region into

235 $1^{\circ} \times 1^{\circ}$ grids (see Fig. S2) for a total 953 grids covering China. Second, we assigned all
236 selected stations to the grids, and this resulted in 627 grids containing stations, which
237 accounted for 65.79% of the total. Finally, the grid box value was the average of all
238 stations in the grid, and the national mean was the area-weight average of all effective
239 grids (Jones and Moberg, 2003).

240 The linear trends reported in this study were calculated via linear regression based
241 on the monthly anomalies of T , R_s , and P . Two national mean trends were calculated
242 from the anomalies of the grids. In the first method (Method I), the national mean
243 monthly anomalies were calculated using the area-weight of each grid first, and then
244 the national mean trend based on the time series of the national average anomalies was
245 calculated. In the second method (Method II), the trend at each grid was calculated first,
246 and then the national mean trend was calculated from the grid trends.

247 In our study, we calculated the national mean trends of the temperatures using
248 Method I and II because both methods have been used in previous studies (Gettelman
249 and Fu, 2008). The results for the two methods are expected to be the same when the
250 time series of all grids is integrated and data are not missing (Zhou et al., 2009);
251 however, when data are missing, small differences may occur (See Table 1). As shown
252 in Table 1, the absolute value of the difference between Method I and Method II ranged

253 from 0.011 to 0.033 °C 10yr⁻¹, which represented 3.4% to 14.3% of the trends (using
254 the results of Method I as the reference). For purposes of clarification, the trends
255 derived from Method I are discussed in the main text, whereas the results from both
256 methods are shown in Table 1.

257 The effect of R_s and P on T_{s-max} and T_{a-max} was determined via a multiple linear
258 regression (Roy and Haigh, 2011) of the monthly anomalies using the following
259 equation:

$$260 \quad T = S_{R_s} \cdot R_s + S_P \cdot P + c + \varepsilon \quad (1)$$

261 where T represents the monthly anomalies of T_{s-max} , T_{s-min} , T_{a-max} , and T_{a-min} ; R_s and P
262 represents the monthly anomalies of surface solar radiation and precipitation
263 respectively. S_{R_s} and S_P are the sensitivities of temperatures to R_s and P , respectively; c
264 is constant term; and ε indicates the residuals of the equation, which represents the
265 contribution from other factors such as longwave radiation flux and internal variability.
266 The coefficients of determination (R^2) for the multilinear regression equation (Eq (1))
267 are shown in Fig. S3, and they indicate the portion of the variance of T that could be
268 attributed to that of R_s and P . High coefficients of determination were obtained, which
269 showed that the linear regression performed well, particularly for South China and the
270 North China Plain. To separate the contributions of R_s and P , we further calculated the

271 partial correlation coefficients between R_s and T (or P and T), which are shown in Fig.
272 S4 and Fig. S5.

273 To determine the effect of R_s and P on the analyzed temperatures, we removed
274 their effects from their original time series of T_{s-max} and T_{a-max} based on the multilinear
275 relationship calculated in Eq (1). Then, we calculated the trends from both the original
276 and adjusted time series. By comparing the derived trends of the original and adjusted
277 time series, we quantitatively assessed the effect of R_s and P on T_{s-max} and T_{a-max} ,
278 particularly for the spatiotemporal pattern of their trends.

279 3. Results

280 3.1. Trends of surface temperature and air temperature

281 3.1.1 Temporal patterns in temperature variability

282 The long-term changes in T_{s-max} and T_{a-max} and T_{s-min} and T_{a-min} from 1960 to
283 2003 are shown in Fig. 2 and Fig. 3, respectively. In addition to the annual variability
284 (Fig. 2a and Fig. 3a), the temperature variability in both warm seasons (May–October;
285 Fig. 2b and Fig. 3b) and cold seasons (November to the following April; Fig. 2c and
286 Fig. 3c) were analyzed. In the annual records, all temperatures exhibited an obvious
287 warming trend throughout China (Fig. 2a and Fig. 3a).

288 As shown in Table 1, the national mean warming rate from 1960 to 2003 for T_{s-}
289 $_{max}$ was 0.227 ± 0.091 °C 10yr^{-1} (95% confidence level) and T_{a-}
290 $_{max}$ was 0.167 ± 0.068 °C 10yr^{-1} (95% confidence level). The warming rate of T_{a-}
291 $_{max}$ based on the 1,977 stations examined in the current study was slightly higher than the global average (0.141 °C
292 10yr^{-1}) from 1950 to 2004 (Vose et al., 2005) and the rate obtained from a previous
293 analysis (0.127 °C 10yr^{-1}) of temperatures from 1955 to 2000 based on 305 stations in
294 China (Liu et al., 2004). Additionally, the increases in T_{s-}
295 $_{max}$ and T_{a-}
296 $_{max}$ in the cold seasons were much larger than those in the warm seasons, which is consistent with
297 previous studies of China and other regions (Vose et al., 2005; Ren et al., 2005; Shen et
al., 2014).

298 Similarly, the warming rates of T_{s-}
299 $_{min}$ and T_{a-}
300 $_{min}$ in the warm seasons were also clearly lower than those in the cold seasons. As shown in Fig. 3, T_{s-}
301 $_{min}$ increased by 0.315 ± 0.058 °C 10yr^{-1} (95% confidence level) and T_{a-}
302 $_{min}$ increased by 0.356 ± 0.057 °C 10yr^{-1} (95% confidence level) (see Fig. 3a) from 1960 to 2003. The warming trend of
303 T_a is generally consistent with earlier studies (Liu et al., 2004; Shen et al., 2014; Li et
304 al., 2015); however, these trends are considerably larger than the rates reported for the
305 global average (0.204 °C 10yr^{-1}) (Vose et al., 2005). For the seasonal scales, the
306 warming rate of T_{s-}
 $_{min}$ and T_{a-}
 $_{min}$ in the cold seasons was almost double that of the warm
seasons from 1960 to 2003 (see Table 1).

307 The warming rate of T_{s-min} (T_{a-min}) was significantly faster than that of T_{s-max} (T_{a-}
308 $-max$) and the warming rates of all temperatures in the cold seasons were substantially
309 greater than those in the warm seasons (Easterling et al., 1997; Liu et al., 2004; Li et
310 al., 2015). Although previous studies have indicated that the microclimate (e.g. urban
311 heat island) has a larger effect on minimum temperatures because of the lower and more
312 stable boundary layer at night (Christy et al., 2009; Zhou and Ren, 2011), many
313 investigators argue that variability in R_s is the primary reason for the daily contrast in
314 warming rates (Makowski et al., 2009; Sanchez-Lorenzo and Wild, 2012).

315 3.1.2. Spatial patterns in temperature variability

316 As shown in Fig. 4, clear spatial heterogeneity was demonstrated in the warming
317 rates for T_{s-max} and T_{a-max} in China from 1960 to 2003. The trends of T_{s-max} and T_{a-max}
318 were statistically higher for the Tibet Plateau, and Northwest and Northeast China (see
319 Fig. S6) compared with the North China Plain and South China. Cooling trends in T_{s-}
320 max even detected for the Sichuan Basin, the Yangtze River Delta, and the Pearl River
321 Delta. Lower rates of warming of T_{a-max} in South China and the North China Plain have
322 also been previously reported (Liu et al., 2004; Li et al., 2015).

323 The warming rates of T_{s-max} and T_{a-max} in South China and the North China Plain
324 in the warm seasons were considerably lower than those in the cold seasons, which

325 resulted in stronger spatial heterogeneity in the warm seasons (Fig. 4b and 4h). The
326 spatial and seasonal patterns of T_{a-max} were similar, although they were not as similar
327 as the patterns of T_{s-max} . The spatial contrast in the trends between T_{s-min} and T_{a-min}
328 was much less than that between T_{s-max} and T_{a-max} , although a strong dependence on
329 latitude was observed (Fig. 4d and 4j). Related studies suggested that this dependence
330 was strongly associated with the mode variability in large-scale circulation, such as a
331 negative trend in the North Atlantic Oscillation during this period (Wallace et al., 2012;
332 Ding et al., 2014).

333 The correlation between T_s and T_a was highly significant. Based on the time series
334 of the national mean yearly anomalies (see Fig. 2 and Fig. 3), the correlation coefficient
335 between T_{s-max} and T_{a-max} was 0.877 and between T_{s-min} and T_{a-min} was 0.976 on the
336 annual scale. In the spatial pattern of the trends (Fig. 4), the correlation coefficient
337 between T_{s-max} and T_{a-max} was 0.488 and between T_{s-min} and T_{a-min} was 0.638 on the
338 annual scale. All of these correlations between T_s and T_a were significant at the 95%
339 significance level, which indicated a close relation between T_s and T_a for both
340 interannual fluctuations and secular trends.

341 The correlation between T_{s-min} and T_{a-min} was significantly higher than that
342 between T_{s-max} and T_{a-max} . T_{s-min} is closely related to the land-atmosphere longwave

343 wave radiation balance at night, which is closely associated with the atmospheric
344 greenhouse effect (Dai et al., 1999). During the day, T_s is directly determined by the
345 land surface energy balance, i.e., the incoming energy (including R_s) and atmospheric
346 longwave radiation (Wang and Dickinson, 2013b), and it is partitioned into latent and
347 sensible heat fluxes (Zhou and Wang, 2016). Although T_a is dependent on the land-
348 atmosphere sensible heat flux, it is also affected by local and/or large-scale circulation.
349 Thus, the changes in the land surface energy balance caused by R_s and P have different
350 levels of effect on T_s and T_a during the day, which most likely caused the lower
351 correlation between T_{s-max} and T_{a-max} than that between T_{s-min} and T_{a-min} .

352 **3.2. Effect of R_s and P on temperatures**

353 **3.2.1 Effect of R_s**

354 As shown in Fig. S4, R_s is closely linked with T_{s-max} and T_{a-max} but not with T_{s-min}
355 and T_{a-min} , and the correlation between T_{s-max} and R_s was higher than that between T_{a-}
356 max and R_s . For the seasonal scales, the partial correlation between T_{s-max} and T_{a-max} and
357 R_s in the warm seasons was higher-stronger than that in the cold seasons, and this
358 correlation was stronger in South China and the North China Plain. South China has
359 high soil moisture; therefore, the relationship between the energy used for
360 evapotranspiration and R_s is approximately linear (Zhou et al., 2007; Wang and

361 Dickinson, 2013a). However, northwest China presents dry soil over most of the year;
362 thus the energy used for evapotranspiration is more dependent on P . As a result, the
363 energy available for heating the surface and air temperatures is not as closely correlated
364 with R_s . Therefore, the correlation coefficients between R_s and T_{s-max} and T_{a-max} were
365 ~~higher~~ lower in ~~South~~ the northwest China.

366 To quantify the effect of R_s on temperature, the sensitivity of the studied
367 temperatures to changes in R_s was calculated (Eq. (1)). As shown in Fig. S7 shows, T_{s-}
368 ~~max~~ was the most sensitive to R_s , followed by T_{a-max} , and the national means for T_{s-max}
369 was $0.092 \pm 0.018 \text{ } ^\circ\text{C (W m}^{-2}\text{)}^{-1}$ (95% confidence level) and T_{a-max} was $0.035 \pm 0.010 \text{ } ^\circ\text{C}$
370 $(\text{W m}^{-2}\text{)}^{-1}$ (95% confidence level). T_{s-min} and T_{a-min} were not sensitive to R_s because
371 these temperatures are primarily affected by atmospheric longwave radiation night.

372 Based on the above analysis, we calculated the effect of changes in R_s on the
373 studied temperatures. From 1960 to 2003, the calculations of the monthly anomalies at
374 1,977 stations indicated that the national mean rate of decrease of R_s was -1.502 ± 0.42
375 $\text{W m}^{-2} 10\text{yr}^{-1}$ (95% confidence level), and the trend was significant in most regions of
376 China (see Fig. S8). Our rate of decrease was considerably less than the global average
377 diminishing rate (from approximately -2.3 to $-5.1 \text{ W m}^{-2} 10\text{yr}^{-1}$) between the 1960s
378 and the 1990s (Gilgen et al., 1998; Stanhill and Cohen, 2001; Liepert, 2002; Ohmura,

379 2006) and the national mean dimming rate across China (from approximately -2.9 to
380 $-5.2 \text{ W m}^{-2} 10\text{yr}^{-1}$) between the 1960s and the 2000s based on radiation station
381 observations (Che et al., 2005; Liang and Xia, 2005; Shi et al., 2008; Wang et al., 2015).

382 As noted in the data section, the sensitivity drift and replacement of instruments
383 used for the R_s observations resulted in a significant homogenization of the station
384 observation records (Wang, 2014; Wang et al., 2015), which introduced considerable
385 uncertainty to the trend estimations. Tang et al. (2011) used quality-controlled
386 observational data from 72 stations and two radiation models based on 479 stations to
387 determine that the rate in China decreased from approximately -2.1 to -2.3 W m^{-2}
388 10yr^{-1} during 1961–2000, and they also showed that R_s values have remained
389 essentially unchanged since 2000. These findings are generally consistent with our
390 results.

391 Because of the decreasing trend in R_s , the national mean warming trends of T_{s-max}
392 and T_{a-max} decreased by $0.139 \text{ }^\circ\text{C } 10\text{yr}^{-1}$ and $0.053 \text{ }^\circ\text{C } 10\text{yr}^{-1}$, respectively. Spatially,
393 the decreasing rate of R_s in South China and the North China Plain was significantly
394 higher than that in other regions, particularly in the warm seasons (Fig. 5b). Therefore,
395 the cooling effect of decreasing R_s on T_{s-max} and T_{a-max} was more significant in South
396 China and the China North Plain, and it resulted in significantly lower warming rates

397 of T_{s-max} and T_{a-max} in those regions than in the other regions (see Fig. 4). The spatial
398 consistency between the decreasing R_s trend and the slowdown of T_{s-max} and T_{a-max}
399 warming implied that variations in R_s were the primary reason for the spatial
400 heterogeneity of the warming rate in T_{s-max} and T_{a-max} .

401 3.2.2 Effect of P

402 As shown in Fig. S5, a significant negative correlation was detected between T_{s-}
403 $_{max}$ and P , and the correlation was more significant in the warm seasons than in the cold
404 seasons. P negatively correlated with temperature because P reduces temperatures by
405 increasing the surface evaporative cooling (Dai et al., 1997; Wang et al., 2006). The
406 national mean sensitivities of T_{s-max} and T_{a-max} to P were -0.321 ± 0.098 °C 10 mm⁻¹
407 and -0.064 ± 0.054 °C 10 mm⁻¹ (95% confidence level), respectively. As shown in Fig.
408 S9, seasonal and spatial changes in the sensitivity of T_{s-max} and T_{a-max} to P were
409 apparent (Fig. S9a–c and Fig. S9g–i). The sensitivities of T_{s-max} and T_{a-max} were
410 significantly higher in arid regions (dry seasons) than humid regions (rainy seasons)
411 (Wang and Dickinson, 2013a). As expected, T_{s-min} and T_{a-min} were both less sensitive
412 to variations in the P .

413 The trend in P from 1960 to 2003 over the 1,977 stations showed obvious spatial
414 heterogeneities. A slight increasing trend in P was observed in China during this period

415 at rate of $0.112 \pm 0.718 \text{ mm } 10\text{yr}^{-1}$ (95% confidence level). An increasing P trend was
416 observed in northwestern China and southeastern China, whereas a decreasing trend
417 was observed in the North China Plain, the Sichuan Basin, and parts of northeastern
418 China. However, the P trends were not significant in most regions (see Fig. S8).
419 Variations in P significantly differed by season (see Fig. 6b and Fig. 6c). The seasonal
420 and spatial variations in P are consistent with those of previous studies (Zhai et al.,
421 2005; Wang et al., 2015).

422 For T_{a-max} and T_{s-max} , the warming trend in the North China Plain, the Sichuan
423 Basin, and parts of northeastern China was aggravated by the reduction in P , whereas
424 the warming trend in northwestern China and in the Mongolian Plateau were slowed by
425 increases in P (Fig. 6d). For the national average, the effect of increasing P resulted in
426 decreases in the warming trends of T_{s-max} and T_{a-max} by $-0.007 \text{ }^\circ\text{C } 10\text{yr}^{-1}$ and $-0.002 \text{ }^\circ\text{C}$
427 10yr^{-1} , respectively. However, the effect of P on T_{s-max} was approximately an order of
428 magnitude less than that of R_s .

429 3.3. Trends of surface and air temperature after adjusting for the effect of R_s and 430 P

431 Based on the above analysis of the effect of R_s and P on temperatures, we found
432 that variations in R_s and P had little effect on T_{s-min} and T_{a-min} . However, R_s and P had

带格式的: 字体: 倾斜

带格式的: 字体: 倾斜

433 important effect on the trends of T_{s-max} and T_{a-max} (see Fig. S3), particularly in central
434 and South China, where ~~T_{s-max} and T_{a-max}~~ ~~T was were~~ more closely related to R_s (see Fig.
435 S4). Therefore, only the effects of R_s and P on T_{s-max} and T_{a-max} were analyzed. After
436 adjusting for the effect of R_s and P (Fig. 7), the warming rates of T_{s-max} and T_{a-max}
437 increased by $0.146\text{ }^{\circ}\text{C}\ 10\text{yr}^{-1}$ (64.3%) and $0.055\text{ }^{\circ}\text{C}\ 10\text{yr}^{-1}$ (33.0%), respectively.
438 Additionally, the increasing amplitude of warming rates in the warm seasons was
439 significantly higher than that in the cold seasons, which resulted in a seasonal contrast
440 in warming rates, with T_{s-max} and T_{a-max} decreasing by 45.0% and 17.2% respectively
441 (see Table 1).

442 More importantly, after adjusting for the effect of R_s and P , the spatial coherence
443 of the warming rates of T_{s-max} and T_{a-max} in South China and the North China Plain
444 clearly improved (Fig. 8). The regional differences among the North China Plain, South
445 China, and other regions in China significantly decreased because of the increase in
446 warming rates in South China and the North China Plain. Additionally, the warming
447 trends of T_{s-max} and T_{a-max} became more statistically significant in the North China
448 Plain and South China (see Fig. S10).

449 To clearly illustrate these changes, we selected two regions in China for further
450 investigation: R1 primarily included the North China Plain and R2 primarily included

451 the Loess Plateau (see Fig. 9a). Although these regions share the same latitudes, the
452 trend for R_s were substantially different (see Fig. 9b). After adjusting for the effect of
453 R_s and P , the annual trends for T_{s-max} and T_{a-max} in R1 increased by 0.304 and 0.118 °C
454 $10yr^{-1}$, respectively, whereas those in R2 increased by only 0.025 and 0.016 °C $10yr^{-1}$,
455 respectively. Therefore, ~~following-after~~ the adjustment, the ~~differences-contrasts~~ in the
456 warming rates of T_{s-max} and T_{a-max} between R1 and R2 were significantly reduced (see
457 Fig. 9d).

458 ~~Following-After~~ the adjustment in R1, the seasonal and diurnal ~~differences~~
459 ~~contrasts~~ in the warming rates of T_{s-max} and T_{a-max} significantly decreased. The
460 ~~contrasts~~~~differences~~ in warming rates between the warm seasons and cold seasons
461 decreased by 68.7% for T_{s-max} and by 50.8% for T_{a-max} after the adjustment.
462 Additionally, the ~~differences-contrasts~~ in the warming rates between T_{s-max} and T_{s-min}
463 decreased by 93.4% and between T_{a-max} and T_{a-min} decreased by 59.6% in R1. In R2,
464 the adjustment did not significantly change the seasonal and diurnal ~~differences~~
465 ~~contrasts~~ in temperatures. Overall, the trends for R1 and R2 became more consistent
466 after adjusting for difference in R_s and P (see Fig. 9d).

467 4. Conclusions and Discussion

468 Although a general warming trends has been observed throughout China, the

469 regional warming trends show significant spatial and temporal heterogeneity. In this
470 study, we analyzed the spatial and temporal patterns of T_s and T_a from 1960 to 2003
471 and further analyzed and quantified the effects of R_s and P on these temperatures. The
472 primary results of the study are as follows.

473 The national mean warming rates from 1960 to 2003 of T_{s-max} , T_{s-min} , T_{a-max} , and
474 T_{a-min} were 0.227 ± 0.091 , 0.315 ± 0.058 , 0.167 ± 0.068 , and 0.356 ± 0.057 °C 10yr^{-1} ,
475 respectively. The warming rates of T_{s-max} and T_{a-max} in South China and the North
476 China Plain were significantly lower than those in the other regions, and the spatial
477 heterogeneity in the warm seasons was greater than that in the cold seasons.

478 During the study period, the R_s value decreased by -1.502 ± 0.042 W m^{-2} 10yr^{-1}
479 (95% confidence level), and higher ~~diminishing-dimming~~ rates were observed in South
480 China and the North China Plain. Using a partial regression analysis, we found that R_s
481 plays a distinctly important role in the spatial warming patterns of T_{s-max} and T_{a-max} .

482 After adjusting for the effect of R_s and P , the warming rates of T_{s-max} and T_{a-max} in
483 South China and the North China Plain significantly increased and the regional
484 differences in warming rates in China clearly decreased (see Fig. 8). After the
485 adjustments, the warming rates of T_{s-max} and T_{a-max} in the North China Plain increased
486 by 0.304 and 0.118 °C 10yr^{-1} , respectively, whereas those on Loess Plateau increased

487 only by 0.025 and 0.016 °C 10yr⁻¹, respectively. Therefore, the differences in warming
488 rates of T_{s-max} and T_{a-max} between the North China Plain and the Loess Plateau were
489 almost eliminated (see Fig. 9d).

490 After adjusting for the effect of R_s and P , the warming trend of T_{s-max} increased by
491 0.146 °C 10yr⁻¹ and that of T_{a-max} increased by 0.055 °C 10yr⁻¹. In addition, the trends
492 of T_{s-max} and T_{a-max} became 0.373 ± 0.068 and 0.222 ± 0.062 °C 10yr⁻¹ respectively.
493 Reduction in R_s resulted in decreases in the warming rates of T_{s-max} and T_{a-max} by
494 0.139 °C 10yr⁻¹ and 0.053 °C 10yr⁻¹, respectively, which accounted for 95.0% and 95.8%
495 of the total effect of R_s and P , respectively. For the seasonal contrast, the warming rates
496 of T_{s-max} and T_{a-max} decreased by 45.0% and 17.2%, respectively. For the daily contrast,
497 the warming rates of T_s and T_a decreased by 33.0% and 29.1%, respectively.

498 In addition to R_s and P , temperature warming rates may be affected by many other
499 factors, such as land cover and land use changes; however those factors have not been
500 discussed in this study because of lack of data (Liu et al., 2005; Zhang et al., 2016).
501 After adjusting for the effect of changes in R_s and P changes, the spatial differences in
502 the warming trends clearly decreased; however, certain regional differences remained.
503 The warming rate of T_{s-max} in the Sichuan Basin remained significantly lower than that
504 in other regions after adjusting for these effects. Additionally, the differences in the

505 warming rates of T_{s-min} and T_{a-min} between the northern and southern areas were not
506 explained by the effects of R_s and P ; further study is required.

507 **Acknowledgements** The National Natural Science Foundation of China (grant no.
508 41525018 and 91337111) and the National Basic Research Program of China funded
509 this study (grant no. 2012CB955302). The land surface temperatures and sunshine
510 duration datasets that include data from approximately 2,400 meteorological stations in
511 China from 1960 to 2003, are obtained from the China Meteorological Administration
512 (CMA, <http://data.cma.gov.cn/data>).

带格式的: 字体: (中文) Times New Roman

513 **References**

- 514 Ait-Mesbah, S., Dufresne, J. L., Cheruy, F., and Hourdin, F.: The role of thermal inertia in the
515 representation of mean and diurnal range of surface temperature in semiarid and arid
516 regions, *Geophys Res Lett*, 42, 7572-7580, 10.1002/2015gl065553, 2015.
- 517 Bounoua, L., Collatz, G. J., Sellers, P. J., Randall, D. A., Dazlich, D. A., Los, S. O., Berry, J.
518 A., Fung, I., Tucker, C. J., Field, C. B., and Jensen, T. G.: Interactions between vegetation
519 and climate: Radiative and physiological effects of doubled atmospheric CO₂, *J Climate*,
520 12, 309-324, 10.1175/1520-0442(1999)012<0309:ibvacr>2.0.co;2, 1999.
- 521 Boyles, R. P., and Raman, S.: Analysis of climate trends in North Carolina (1949-1998),
522 *Environ Int*, 29, 263-275, 10.1016/s0160-4120(02)00185-x, 2003.
- 523 Campbell, G. G., and VonderHaar, T. H.: Comparison of surface temperature minimum and
524 maximum and satellite measured cloudiness and radiation budget, *J Geophys Res-Atmos*,
525 102, 16639-16645, 10.1029/96jd02718, 1997.
- 526 Cao, L., Zhu, Y., Tang, G., Yuan, F., and Yan, Z.: Climatic warming in China according to a
527 homogenized data set from 2419 stations, *Int J Climatol*, 36, 4384-4392, 10.1002/joc.4639,
528 2016.
- 529 Che, H. Z., Shi, G. Y., Zhang, X. Y., Arimoto, R., Zhao, J. Q., Xu, L., Wang, B., and Chen, Z.
530 H.: Analysis of 40 years of solar radiation data from China, 1961-2000, *Geophys Res Lett*,
531 32, L06803, 10.1029/2004gl022322, 2005.
- 532 Chen, H. S., Ma, H. D., Li, X., and Sun, S. L.: Solar influences on spatial patterns of Eurasian
533 winter temperature and atmospheric general circulation anomalies, *J Geophys Res-Atmos*,
534 120, 8642-8657, 10.1002/2015jd023415, 2015.
- 535 Cheng, Z., Wang, S., Fu, X., Watson, J. G., Jiang, J., Fu, Q., Chen, C., Xu, B., Yu, J., Chow, J.
536 C., and Hao, J.: Impact of biomass burning on haze pollution in the Yangtze River delta,
537 China: a case study in summer 2011, *Atmos. Chem. Phys.*, 14, 4573-4585, 10.5194/acp-
538 14-4573-2014, 2014.
- 539 Christy, J. R., Norris, W. B., and McNider, R. T.: Surface Temperature Variations in East Africa
540 and Possible Causes, *J Climate*, 22, 3342-3356, 10.1175/2008jcli2726.1, 2009.

带格式的: 缩进: 左侧: 0 厘米, 悬挂缩进: 2 字符, 首行缩进: -2 字符

- 541 Dai, A., DelGenio, A. D., and Fung, I. Y.: Clouds, precipitation and temperature range, *Nature*,
542 386, 665-666, 10.1038/386665b0, 1997.
- 543 Dai, A., Trenberth, K. E., and Karl, T. R.: Effects of clouds, soil moisture, precipitation, and
544 water vapor on diurnal temperature range, *J Climate*, 12, 2451-2473, 10.1175/1520-
545 0442(1999)012<2451:eocsmg>2.0.co;2, 1999.
- 546 Ding, Q., Wallace, J. M., Battisti, D. S., Steig, E. J., Gallant, A. J. E., Kim, H.-J., and Geng, L.:
547 Tropical forcing of the recent rapid Arctic warming in northeastern Canada and Greenland,
548 *Nature*, 509, 209-212, 10.1038/nature13260, 2014.
- 549 Duan, A., and Xiao, Z.: Does the climate warming hiatus exist over the Tibetan Plateau?, *Sci.*
550 *Rep.* 5, 13711, 10.1038/srep13711, 2015.
- 551 Easterling, D. R., Horton, B., Jones, P. D., Peterson, T. C., Karl, T. R., Parker, D. E., Salinger,
552 M. J., Razuvayev, V., Plummer, N., Jamason, P., and Folland, C. K.: Maximum and
553 minimum temperature trends for the globe, *Science*, 277, 364-367,
554 10.1126/science.277.5324.364, 1997.
- 555 Falge, E., Reth, S., Bruggemann, N., Butterbach-Bahl, K., Goldberg, V., Oltchev, A., Schaaf,
556 S., Spindler, G., Stiller, B., Queck, R., Kostner, B., and Bernhofer, C.: Comparison of
557 surface energy exchange models with eddy flux data in forest and grassland ecosystems
558 of Germany, *Ecol Model*, 188, 174-216, 10.1016/j.ecolmodel.2005.01.057, 2005.
- 559 Gettelman, A., and Fu, Q.: Observed and simulated upper-tropospheric water vapor feedback,
560 *J Climate*, 21, 3282-3289, 10.1175/2007jcli2142.1, 2008.
- 561 Gilgen, H., Wild, M., and Ohmura, A.: Means and trends of shortwave irradiance at the surface
562 estimated from global energy balance archive data, *J Climate*, 11, 2042-2061,
563 10.1175/1520-0442-11.8.2042, 1998.
- 564 Hartmann, D. L., Ramanathan, V., Berroir, A., and Hunt, G. E.: Earth radiation budget data and
565 climate research, *Rev Geophys*, 24, 439-468, 10.1029/RG024i002p00439, 1986.
- 566 Hartmann, D. L., Tank, A. M. G. K., and Rusticucci, M.: Observation: Atmosphere and surface,
567 IPCC, 161-218, 10.1017/CBO9781107415324, 2013.
- 568 Hegerl, G. C., and Zwiers, F. W.: Climate change 2007: Understanding and attributing climate
569 change, IPCC, 665-744, 10.1017/CBO9781107415324, 2007.

- 570 Hingray, B., Mezghani, A., and Buishand, T. A.: Development of probability distributions for
571 regional climate change from uncertain global mean warming and an uncertain scaling
572 relationship, *Hydrol Earth Syst Sc*, 11, 1097-1114, 10.5194/hess-11-1097-2007, 2007.
- 573 Huang, J., Guan, X., and Ji, F.: Enhanced cold-season warming in semi-arid regions, *Atmos.*
574 *Chem. Phys.*, 12, 5391-5398, 10.5194/acp-12-5391-2012, 2012.
- 575 Jones, P. D., and Moberg, A.: Hemispheric and large-scale surface air temperature variations:
576 An extensive revision and an update to 2001, *J Climate*, 16, 206-223, 10.1175/1520-
577 0442(2003)016<0206:halssa>2.0.co;2, 2003.
- 578 Kalnay, E., and Cai, M.: Impact of urbanization and land-use change on climate, *Nature*, 423,
579 528-531, 10.1038/nature01675, 2003.
- 580 Karl, T. R., Kukla, G., Razuvayev, V. N., Changery, M. J., Quayle, R. G., Heim, R. R.,
581 Easterling, D. R., and Fu, C. B.: Global warming - evidence for asymmetric diurnal
582 temperature-change, *Geophys Res Lett*, 18, 2253-2256, 10.1029/91gl02900, 1991.
- 583 Karoly, D. J., and Stott, P. A.: Anthropogenic warming of central England temperature, *Atmos.*
584 *Sci. Lett.*, 7, 81-85, 10.1002/asl.136, 2006.
- 585 Kukla, G., and Karl, T. R.: Nighttime warming and the greenhouse-effect, *Environ Sci Technol*,
586 27, 1468-1474, 10.1021/es00045a001, 1993.
- 587 Lauritsen, R. G., and Rogers, J. C.: US Diurnal Temperature Range Variability and Regional
588 Causal Mechanisms, 1901-2002, *J Climate*, 25, 7216-7231, 10.1175/jcli-d-11-00429.1,
589 2012.
- 590 Li, B. F., Chen, Y. N., and Shi, X.: Why does the temperature rise faster in the arid region of
591 northwest China?, *J Geophys Res-Atmos*, 117, D16115, 10.1029/2012jd017953, 2012.
- 592 Li, Q. X., Yang, S., Xu, W. H., Wang, X. L. L., Jones, P., Parker, D., Zhou, L. M., Feng, Y., and
593 Gao, Y.: China experiencing the recent warming hiatus, *Geophys Res Lett*, 42, 889-898,
594 10.1002/2014gl062773, 2015.
- 595 Liang, F., and Xia, X. A.: Long-term trends in solar radiation and the associated climatic factors
596 over China for 1961-2000, *Ann Geophys*, 23, 2425-2432, 10.5194/angeo-23-2425-2005,
597 2005.

- 598 Liepert, B. G.: Observed reductions of surface solar radiation at sites in the United States and
599 worldwide from 1961 to 1990, *Geophys Res Lett*, 29, 1421, 10.1029/2002gl014910, 2002.
- 600 Lim, Y. K., Cai, M., Kalnay, E., and Zhou, L. M.: Observational evidence of sensitivity of
601 surface climate changes to land types and urbanization, *Geophys Res Lett*, 32, L22712,
602 10.1029/2005gl024267, 2005.
- 603 Liu, B. H., Xu, M., Henderson, M., Qi, Y., and Li, Y. Q.: Taking China's temperature: Daily
604 range, warming trends, and regional variations, 1955-2000, *J Climate*, 17, 4453-4462,
605 10.1175/3230.1, 2004.
- 606 Liu, J. Y., Liu, M. L., Tian, H. Q., Zhuang, D. F., Zhang, Z. X., Zhang, W., Tang, X. M., and
607 Deng, X. Z.: Spatial and temporal patterns of China's cropland during 1990-2000: An
608 analysis based on Landsat TM data, *Remote Sens Environ*, 98, 442-456,
609 10.1016/j.rse.2005.08.012, 2005.
- 610 Mahlstein, I., and Knutti, R.: Regional climate change patterns identified by cluster analysis,
611 *Clim Dynam*, 35, 587-600, 10.1007/s00382-009-0654-0, 2010.
- 612 Makowski, K., Jaeger, E. B., Chiacchio, M., Wild, M., Ewen, T., and Ohmura, A.: On the
613 relationship between diurnal temperature range and surface solar radiation in Europe, *J*
614 *Geophys Res-Atmos*, 114, D00D07, 10.1029/2008JD011104, 2009.
- 615 Manara, V., Beltrano, M. C., Brunetti, M., Maugeri, M., Sanchez-Lorenzo, A., Simolo, C., and
616 Sorrenti, S.: Sunshine duration variability and trends in Italy from homogenized
617 instrumental time series (1936-2013), *J Geophys Res-Atmos*, 120, 3622-3641,
618 10.1002/2014jd022560, 2015.
- 619 Mariotti, L., Coppola, E., Sylla, M. B., Giorgi, F., and Piani, C.: Regional climate model
620 simulation of projected 21st century climate change over an all-Africa domain:
621 Comparison analysis of nested and driving model results, *J Geophys Res-Atmos*, 116,
622 D15111, 10.1029/2010jd015068, 2011.
- 623 Menon, S., Hansen, J., Nazarenko, L., and Luo, Y. F.: Climate effects of black carbon aerosols
624 in China and India, *Science*, 297, 2250-2253, 10.1126/science.1075159, 2002.
- 625 Ohmura, A.: Observed long-term variations of solar irradiance at the earth's surface, *Space Sci*
626 *Rev*, 125, 111-128, 10.1007/s11214-006-9050-9, 2006.

- 627 Peng, S. S., Piao, S. L., Zeng, Z. Z., Ciais, P., Zhou, L. M., Li, L. Z. X., Myneni, R. B., Yin, Y.,
628 and Zeng, H.: Afforestation in China cools local land surface temperature, *P Natl Acad Sci*
629 *USA*, 111, 2915-2919, 10.1073/pnas.1315126111, 2014.
- 630 Ren, G., Xu, M., Chu, Z., Guo, J., Li, Q., Liu, X., and Wang, Y.: Changes of Surface Air
631 Temperature in China During 1951-2004, *Climatic and environmental research*, 10, 717-
632 727, 2005.
- 633 Roy, I., and Haigh, J. D.: The influence of solar variability and the quasi-biennial oscillation on
634 lower atmospheric temperatures and sea level pressure, *Atmos. Chem. Phys.*, 11, 11679-
635 11687, 10.5194/acp-11-11679-2011, 2011.
- 636 Sanchez-Lorenzo, A., and Wild, M.: Decadal variations in estimated surface solar radiation
637 over Switzerland since the late 19th century, *Atmos. Chem. Phys.*, 12, 8635-8644,
638 10.5194/acp-12-8635-2012, 2012.
- 639 Seneviratne, S. I., Corti, T., Davin, E. L., Hirschi, M., Jaeger, E. B., Lehner, I., Orlowsky, B.,
640 and Teuling, A. J.: Investigating soil moisture-climate interactions in a changing climate:
641 A review, *Earth-sci Rev*, 99, 125-161, 10.1016/j.earscirev.2010.02.004, 2010.
- 642 Shen, D. J., and Varis, O.: Climate change in China, *Ambio*, 30, 381-383, 10.1639/0044-
643 7447(2001)030[0381:ccic]2.0.co;2, 2001.
- 644 Shen, M. G., Piao, S. L., Jeong, S. J., Zhou, L. M., Zeng, Z. Z., Ciais, P., Chen, D. L., Huang,
645 M. T., Jin, C. S., Li, L. Z. X., Li, Y., Myneni, R. B., Yang, K., Zhang, G. X., Zhang, Y. J.,
646 and Yao, T. D.: Evaporative cooling over the Tibetan Plateau induced by vegetation growth,
647 *P Natl Acad Sci USA*, 112, 9299-9304, 10.1073/pnas.1504418112, 2015.
- 648 Shen, X. J., Liu, B. H., Li, G. D., Wu, Z. F., Jin, Y. H., Yu, P. J., and Zhou, D. W.: Spatiotemporal
649 change of diurnal temperature range and its relationship with sunshine duration and
650 precipitation in China, *J Geophys Res-Atmos*, 119, 13163-13179, 10.1002/2014jd022326,
651 2014.
- 652 Shi, G. Y., Hayasaka, T., Ohmura, A., Chen, Z. H., Wang, B., Zhao, J. Q., Che, H. Z., and Xu,
653 L.: Data quality assessment and the long-term trend of ground solar radiation in China, *J*
654 *Appl. Meteorol. Clim.*, 47, 1006-1016, 10.1175/2007jamc1493.1, 2008.
- 655 Stanhill, G., and Cohen, S.: Global dimming: a review of the evidence for a widespread and
656 significant reduction in global radiation with discussion of its probable causes and possible

- 657 agricultural consequences, *Agr Forest Meteorol*, 107, 255-278, 10.1016/s0168-
658 1923(00)00241-0, 2001.
- 659 Sun, Y., Zhang, X. B., Ren, G. Y., Zwiers, F. W., and Hu, T.: Contribution of urbanization to
660 warming in China, *Nature Climate Change*, 6, 706-709, 10.1038/nclimate2956, 2016.
- 661 Tang, W. J., Yang, K., Qin, J., Cheng, C. C. K., and He, J.: Solar radiation trend across China
662 in recent decades: a revisit with quality-controlled data, *Atmos. Chem. Phys.*, 11, 393-406,
663 10.5194/acp-11-393-2011, 2011.
- 664 Taylor, J. R., Randel, W. J., and Jensen, E. J.: Cirrus cloud-temperature interactions in the
665 tropical tropopause layer: a case study, *Atmos. Chem. Phys.*, 11, 10085-10095,
666 10.5194/acp-11-10085-2011, 2011.
- 667 Tebaldi, C., Smith, R. L., Nychka, D., and Mearns, L. O.: Quantifying uncertainty in projections
668 of regional climate change: A Bayesian approach (vol 18, pg 1524, 2005), *J Climate*, 18,
669 3405-3405, 10.1175/JCLI9001.1a, 2005.
- 670 Vautard, R., Yiou, P., and van Oldenborgh, G. J.: Decline of fog, mist and haze in Europe over
671 the past 30 years, *Nat Geosci*, 2, 115-119, 10.1038/ngeo414, 2009.
- 672 Vose, R. S., Easterling, D. R., and Gleason, B.: Maximum and minimum temperature trends for
673 the globe: An update through 2004, *Geophys Res Lett*, 32, L23822,
674 10.1029/2005gl024379, 2005.
- 675 Wallace, J. M., Fu, Q., Smoliak, B. V., Lin, P., and Johanson, C. M.: Simulated versus observed
676 patterns of warming over the extratropical Northern Hemisphere continents during the
677 cold season, *P Natl Acad Sci USA*, 109, 14337-14342, 10.1073/pnas.1204875109, 2012.
- 678 Wang, K., Dickinson, R. E., Wild, M., and Liang, S.: Evidence for decadal variation in global
679 terrestrial evapotranspiration between 1982 and 2002: 1. Model development, *J Geophys
680 Res-Atmos*, 115, D20112, 10.1029/2010JD013847, 2010a.
- 681 Wang, K., Dickinson, R. E., Wild, M., and Liang, S.: Evidence for decadal variation in global
682 terrestrial evapotranspiration between 1982 and 2002: 2. Results, *J Geophys Res-Atmos*,
683 115, D20113, 10.1029/2009JD013671, 2010b.
- 684 Wang, K., and Dickinson, R. E.: Contribution of solar radiation to decadal temperature
685 variability over land, *P Natl Acad Sci USA*, 110, 14877-14882, 10.1073/pnas.1311433110,

686 2013a.

687 Wang, K., and Dickinson, R. E.: Global atmospheric downward longwave radiation at the
688 surface from ground-based observations, satellite retrievals, and reanalyses, *Rev Geophys*,
689 51, 150-185, 10.1002/rog.20009, 2013b.

690 Wang, K., Ma, Q., Li, Z., and Wang, J.: Decadal variability of surface incident solar radiation
691 over China: Observations, satellite retrievals, and reanalyses, *J Geophys Res-Atmos*, 120,
692 6500-6514, 10.1002/2015jd023420, 2015.

693 Wang, K. C., Li, Z. Q., and Cribb, M.: Estimation of evaporative fraction from a combination
694 of day and night land surface temperatures and NDVI: A new method to determine the
695 Priestley-Taylor parameter, *Remote Sens Environ*, 102, 293-305,
696 10.1016/j.rse.2006.02.007, 2006.

697 Wang, K. C., and Liang, S. L.: Estimation of Daytime Net Radiation from Shortwave Radiation
698 Measurements and Meteorological Observations, *J. Appl. Meteorol. Clim.*, 48, 634-643,
699 10.1175/2008jamc1959.1, 2008.

700 Wang, K. C., and Dickinson, R. E.: A review of global terrestrial evapotranspiration:
701 Observation, modeling, climatology, and climatic variability, *Rev Geophys*, 50, RG2005,
702 10.1029/2011rg000373, 2012.

703 Wang, K. C., Dickinson, R. E., Wild, M., and Liang, S.: Atmospheric impacts on climatic
704 variability of surface incident solar radiation, *Atmos. Chem. Phys.*, 12, 9581-9592,
705 10.5194/acp-12-9581-2012, 2012.

706 Wang, K. C.: Measurement Biases Explain Discrepancies between the Observed and Simulated
707 Decadal Variability of Surface Incident Solar Radiation, *Sci. Rep*, 4, 6144,
708 10.1038/srep06144, 2014.

709 Wang, K. C., and Zhou, C. L. E.: Regional Contrasts of the Warming Rate over Land
710 Significantly Depend on the Calculation Methods of Mean Air Temperature, *Sci. Rep*, 5,
711 12324, 10.1038/srep12324, 2015.

712 Wang, X., Wang, K., and Su, L.: Contribution of Atmospheric Diffusion Conditions to the
713 Recent Improvement in Air Quality in China, *Sci. Rep*, 6, 36404, 10.1038/srep36404,
714 2016.

- 715 Weng, Q. H., Lu, D. S., and Schubring, J.: Estimation of land surface temperature-vegetation
716 abundance relationship for urban heat island studies, *Remote Sens Environ*, 89, 467-483,
717 10.1016/j.rse.2003.11.005, 2004.
- 718 Wild, M., Ohmura, A., and Makowski, K.: Impact of global dimming and brightening on global
719 warming, *Geophys Res Lett*, 34, L04702, 10.1029/2006gl028031, 2007.
- 720 Wild, M.: Enlightening global dimming and brightening, *B Am Meteorol Soc*, 93, 27-37,
721 10.1175/bams-d-11-00074.1, 2012.
- 722 Xia, X.: A closer looking at dimming and brightening in China during 1961-2005, *Ann Geophys*,
723 28, 1121-1132, 10.5194/angeo-28-1121-2010, 2010.
- 724 Yang, K., Koike, T., and Ye, B. S.: Improving estimation of hourly, daily, and monthly solar
725 radiation by importing global data sets, *Agr Forest Meteorol*, 137, 43-55,
726 10.1016/j.agrformet.2006.02.001, 2006.
- 727 Yin, Z., Wang, H., and Chen, H.: Understanding Severe Winter Haze Pollution in the North-
728 Central North China Plain in 2014, *Atmos. Chem. Phys.*, 17, 1641-1651, 10.5194/acp-
729 2016-641, 2017.
- 730 You, Q. L., Min, J. Z., Jiao, Y., Sillanpaa, M., and Kang, S. C.: Observed trend of diurnal
731 temperature range in the Tibetan Plateau in recent decades, *Int J Climatol*, 36, 2633-2643,
732 10.1002/joc.4517, 2016.
- 733 Zhai, P. M., Zhang, X. B., Wan, H., and Pan, X. H.: Trends in total precipitation and frequency
734 of daily precipitation extremes over China, *J Climate*, 18, 1096-1108, 10.1175/jcli-3318.1,
735 2005.
- 736 Zhang, X., Sun, Y., Mao, W., Liu, Y., and Ren, Y.: Regional Response of Temperature Change
737 in the Arid Regions of China to Global Warming, *Arid Zone Research*, 27, 592-599, 2010.
- 738 Zhang, Z. X., Li, N., Wang, X., Liu, F., and Yang, L. P.: A Comparative Study of Urban
739 Expansion in Beijing, Tianjin and Tangshan from the 1970s to 2013, *Remote. Sen.*, 8, 496,
740 10.3390/rs8060496, 2016.
- 741 Zhou, C. L., and Wang, K. C.: Coldest Temperature Extreme Monotonically Increased and
742 Hottest Extreme Oscillated over Northern Hemisphere Land during Last 114 Years, *Sci.*
743 *Rep.*, 6, 25721, 10.1038/srep25721, 2016.

744 Zhou, L. M., Dickinson, R. E., Tian, Y. H., Fang, J. Y., Li, Q. X., Kaufmann, R. K., Tucker, C.
745 J., and Myneni, R. B.: Evidence for a significant urbanization effect on climate in China,
746 P Natl Acad Sci USA, 101, 9540-9544, 10.1073/pnas.0400357101, 2004.

747 Zhou, L. M., Dickinson, R. E., Tian, Y. H., Vose, R. S., and Dai, Y. J.: Impact of vegetation
748 removal and soil aridation on diurnal temperature range in a semiarid region: Application
749 to the Sahel, P Natl Acad Sci USA, 104, 17937-17942, 10.1073/pnas.0700290104, 2007.

750 Zhou, L. M., Dai, A., Dai, Y. J., Vose, R., Zou, C. Z., Tian, Y. H., and Chen, H. S.: Spatial
751 dependence of diurnal temperature range trends on precipitation from 1950 to 2004, Clim
752 Dynam, 32, 429-440, 10.1007/s00382-008-0387-5, 2009.

753 Zhou, L. M., Dickinson, R. E., Dai, A. G., and Dirmeyer, P.: Detection and attribution of
754 anthropogenic forcing to diurnal temperature range changes from 1950 to 1999:
755 comparing multi-model simulations with observations, Clim Dynam, 35, 1289-1307,
756 10.1007/s00382-009-0644-2, 2010.

757 Zhou, Y. Q., and Ren, G. Y.: Change in extreme temperature event frequency over mainland
758 China, 1961-2008, Climate Res, 50, 125-139, 10.3354/cr01053, 2011.

759

760

761

762

763

764

带格式的: 缩进: 左侧: 0 厘米, 悬挂缩进: 2 字符, 首行缩进: -2 字符, 定义网格后不调整右缩进

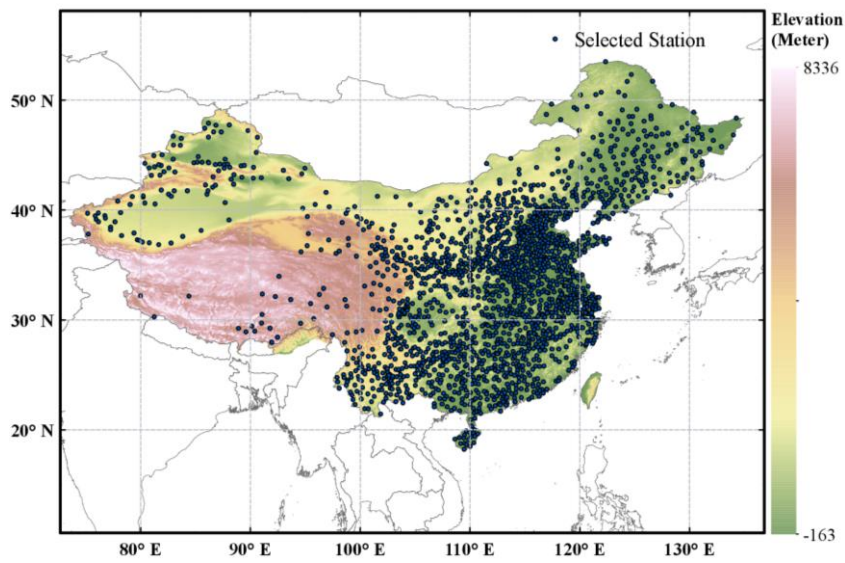
带格式的: 缩进: 左侧: 0 厘米, 悬挂缩进: 2 字符, 首行缩进: -2 字符, 定义网格后不调整右缩进

765

766

767

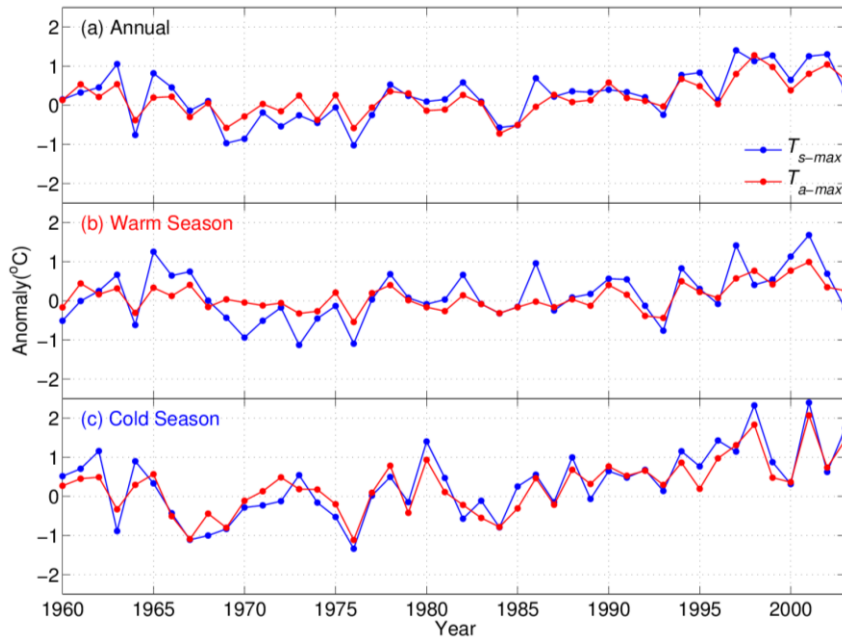
带格式的: 缩进: 左侧: 0 厘米, 悬挂缩进: 2 字符, 首行缩进: -2 字符, 定义网格后不调整右缩进



768

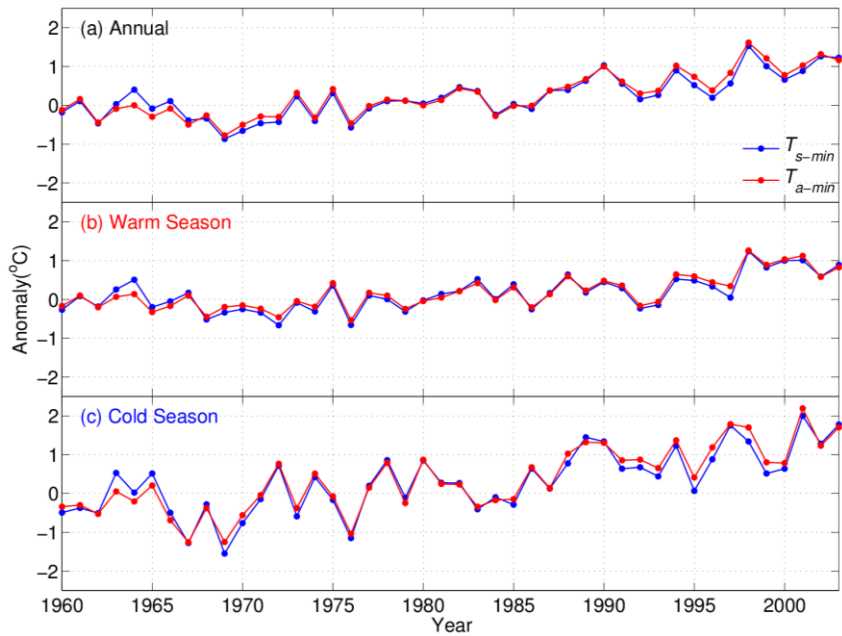
769 Figure 1. Elevation maps of mainland China and spatial distribution of the 1977
770 meteorological stations used in this study. The datasets were provided by China's
771 National Meteorological Information Centre (You et al., 2016)
772 (<http://data.cma.gov.cn/data>).

773



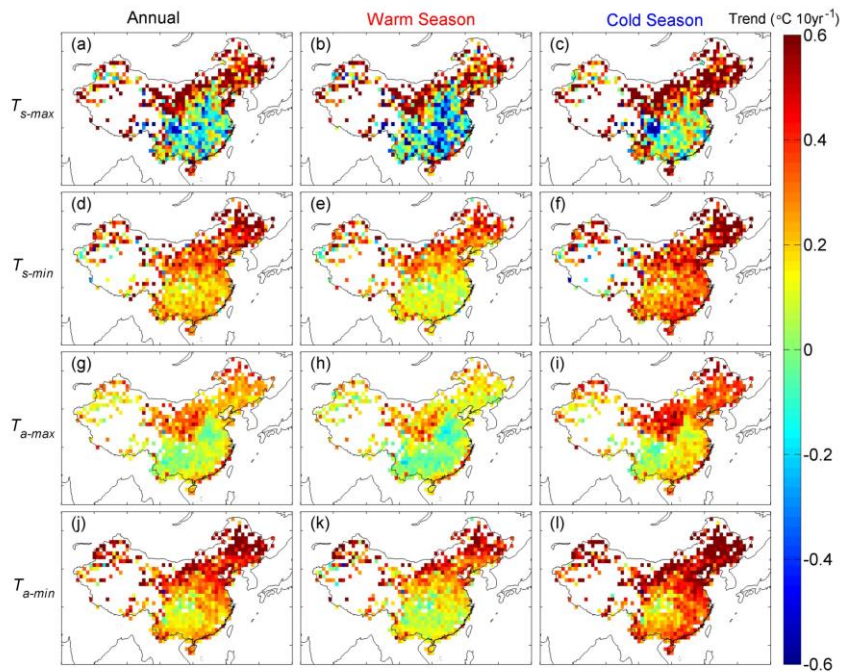
774

775 Figure 2. National mean yearly anomalies of daily maximum land surface temperature
 776 (T_{s-max} , blue line) and daily maximum air temperature (T_{a-max} , red line) for the annual
 777 (a), warm (b), and cold (c) seasonal scales for the reference period from 1961 to 1990.



778

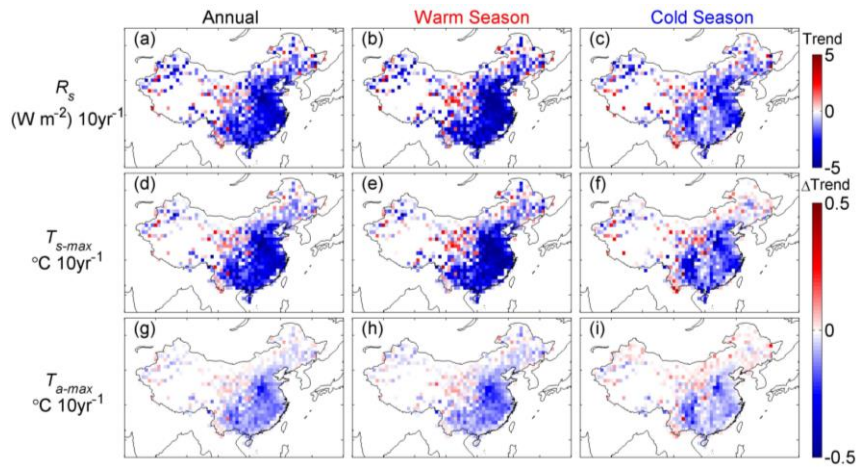
779 Figure 3. National mean yearly anomalies of daily minimum land surface temperature
 780 (T_{s-min} , blue line) and daily minimum air temperature (T_{a-min} , red line) for the annual
 781 (a), warm (b), and cold (c) seasonal scales for the reference period 1961–1990.



782

783 Figure 4. Maps of the trends of the monthly anomalies for daily maximum land surface
 784 temperature (T_{s-max} , a-c), daily minimum land surface temperature (T_{s-min} , d-f), daily
 785 maximum air temperature (T_{a-max} , g-i), and daily minimum air temperature (T_{a-min} , j-
 786 l) for the annual, warm (May-October), and cold (November-next April) seasonal
 787 scales. All trends reported in these figures were calculated using a linear regression
 788 based on the least square method.

789

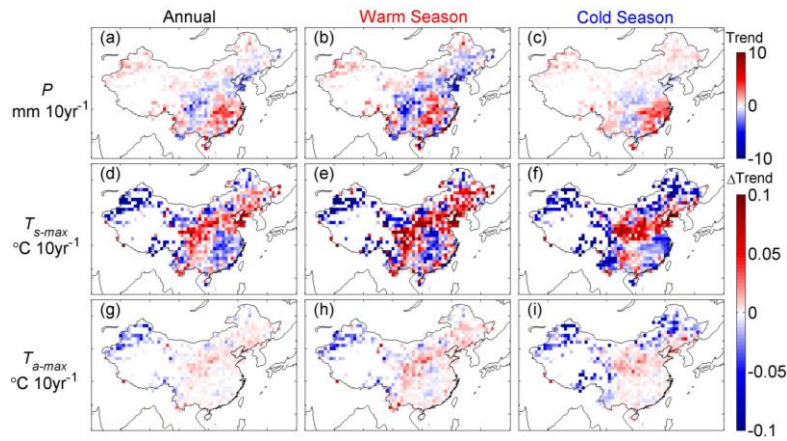


790

791 Figure 5. Maps of the trends in surface solar radiation (R_s , a–c) and its effect on the
 792 warming rates of daily maximum land surface temperature (T_{s-max} , d–f) and daily
 793 maximum air temperature (T_{a-max} , g–i). The first line (a–c) is the trend of R_s from
 794 1960–2003; the second line (d–f) and the third line (g–i) are the trend changes caused
 795 by secular variations of R_s on T_{s-max} and T_{a-max} . Eq (1) was used to strip away the effect
 796 of R_s on temperatures, and we calculated the trend difference (Δ Trend, d–i) between
 797 the time series of temperatures before and after adjusting for the effect of R_s . Finally,
 798 the effect of R_s on the trends of T_{s-max} and T_{a-max} was quantified and analyzed (section
 799 3.2.1).

800

801

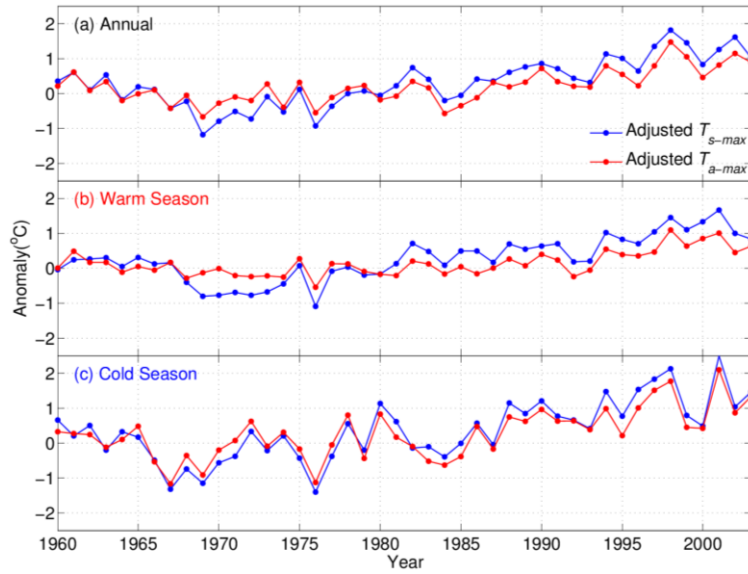


802

803 Figure 6. Maps of the trends in precipitation (P) (a–c) and their effect on the warming
 804 rates for daily maximum land surface temperature (T_{s-max} , d–f) and daily maximum air
 805 temperature (T_{a-max} , g–i). The first line (a–c) is the trend of P during 1960–2003; the
 806 second line (d–f) and the third line (g–i) are the trend changes caused by secular
 807 variations of P on T_{s-max} and T_{a-max} . We used Eq (1) to remove the effects of P on the
 808 temperatures, then calculated the trend difference (Δ Trend, d–i) between the time series
 809 of temperatures before and after adjusting for the effect of P . Finally, the effect of P on
 810 the trends of T_{s-max} and T_{a-max} was quantified and analyzed (section 3.2.2).

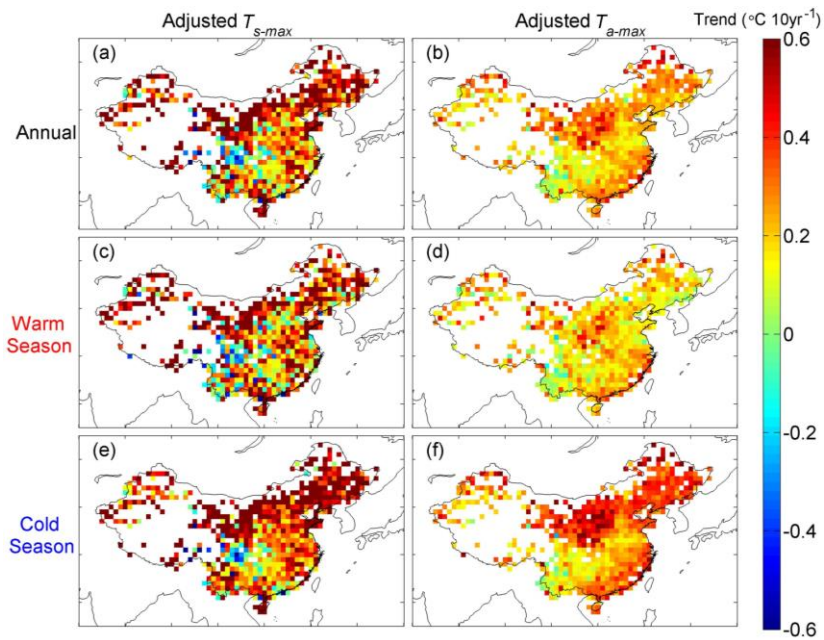
811

812



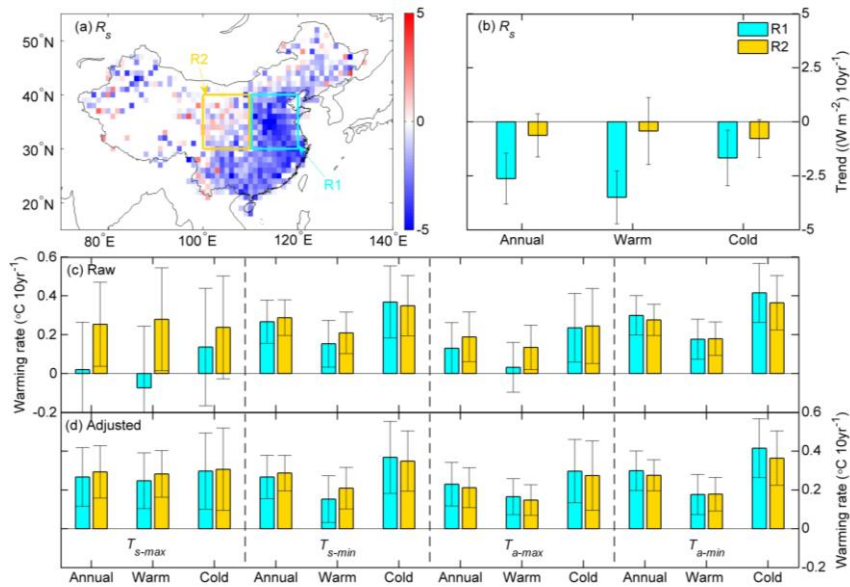
813

814 Figure 7. Regional average anomalies of daily maximum land surface temperature (T_{s-}
 815 max , blue line) and daily maximum air temperature (T_{a-max} , red line) for the annual (a),
 816 warm (b), and cold (c) seasonal scales for the reference period from 1961 to 1990. We
 817 used Eq (1) to simultaneously adjust for the effects of surface solar radiation (R_s) and
 818 precipitation (P) on T_{s-max} and T_{a-max} and then analyzed the changes in the interannual
 819 variation of T_{s-max} and T_{a-max} (section 3.3).



820

821 Figure 8. Maps of the trends of the monthly anomalies for the daily maximum land
 822 surface temperature (T_{s-max} , a, c, e) and daily maximum air temperature (T_{a-max} , b, d, f)
 823 for the annual, warm, and cold seasonal scales after adjusting for the effects of surface
 824 solar radiation (R_s) and precipitation (P). We used Eq (1) to simultaneously adjust the
 825 effects of R_s and P on T_{s-max} and T_{a-max} and then analyzed the changes in the secular
 826 trends of T_{s-max} and T_{a-max} (section 3.3).



827

828 Figure 9. (a) Maps of the trends of surface solar radiation (R_s) and the location of the
 829 regions selected for further analysis: R1 (latitude: 30°—40° N; longitude: 110°—120°
 830 W) and R2 (latitude: 30°—40° N; longitude: 100°—110° W). (b) National mean trends
 831 for R1 and R2. (c) Annual, warm, and cold seasonal scale trends calculated based on
 832 the data before adjusting the effect of R_s and P . (d) Annual, warm, and cold seasonal
 833 scale trends calculated based on the data after adjusting the effect of R_s and P . All error
 834 bars indicate the 95% confidence interval.

835

836

837

838 Table 1. Warming rates (unit: °C 10yr⁻¹) of the temperatures (T_{s-max} , T_{s-min} , T_{a-max} , T_{a-min})
839 for the annual, warm and cold seasonal scales. Raw and Adjusted represent the warming
840 rates calculated for the data before and after adjusting for the effect of surface solar
841 radiation (R_s) and precipitation (P), respectively. In Method I, the national mean
842 anomalies were calculated first and then the national mean trend based on this time
843 series was calculated. In Method II, the trend of each grid was calculated first and then
844 the national mean value of the trends of all grids was calculated using the area-weight
845 average method. We calculated the national mean trends of the temperatures using both
846 methods.

		T_{s-max}	T_{s-min}	T_{a-max}	T_{a-min}	
Method I	Raw	Annual	0.227±0.091	0.315±0.058	0.167±0.068	0.356±0.057
		Warm	0.172±0.103	0.221±0.054	0.091±0.056	0.245±0.049
		Cold	0.354±0.149	0.447±0.101	0.294±0.123	0.505±0.098
	Adjusted	Annual	0.373±0.068	--	0.222±0.062	--
		Warm	0.350±0.064	--	0.160±0.046	--
		Cold	0.450±0.119	--	0.329±0.114	--
Method II	Raw	Annual	0.254±0.197	0.328±0.094	0.183±0.103	0.368±0.082
		Warm	0.193±0.285	0.235±0.095	0.104±0.109	0.256±0.081
		Cold	0.321±0.267	0.415±0.159	0.264±0.167	0.476±0.139
	Adjusted	Annual	0.401±0.137	--	0.239±0.086	--
		Warm	0.374±0.173	--	0.174±0.082	--
		Cold	0.432±0.208	--	0.304±0.152	--

Units: °C 10yr⁻¹, ±95% Confidence interval.

847

848